NeuroImage 44 (2009) 1334–1344

Contents lists available at ScienceDirect

NeuroImage

journal homepage: www.elsevier.com/locate/ynimg

The distribution of D2/D3 receptor binding in the adolescent rhesus monkey using small animal PET imaging

Bradley T. Christian *, Nicholas T. Vandehey, Andrew S. Fox, Dhanabalan Murali, Terrence R. Oakes, Alex K. Converse, Robert J. Nickles, Steve E. Shelton, Richard J. Davidson, Ned H. Kalin

Department of Psychiatry, University of Wisconsin-Madison, USA
Department of Medical Physics, University of Wisconsin-Madison, USA
Harlow Primate Center, University of Wisconsin-Madison, USA
Waisman Laboratory for Brain Imaging and Behavior, University of Wisconsin-Madison, USA

ARTICLE INFO

Article history:
Received 1 July 2008
Revised 9 October 2008
Accepted 12 October 2008
Available online 29 October 2008

ABSTRACT

PET imaging of the neuroreceptor systems in the brain has earned a prominent role in studying normal development, neuropsychiatric illness and developing targeted drugs. The dopaminergic system is of particular interest due to its role in the development of cognitive function and mood as well as its suspected involvement in neuropsychiatric illness. Nonhuman primate animal models provide a valuable resource for relating neurochemical changes to behavior. To facilitate comparison within and between primate models, we report *in vivo* D2/D3 binding in a large cohort of adolescent rhesus monkeys. **Methods:** In this work, the *in vivo* D2/D3 dopamine receptor availability was measured in a cohort of 33 rhesus monkeys in the adolescent stage of development (3.2–5.3 years). Both striatal and extrastriatal D2/D3 binding were measured using [F-18]fallypride with a high resolution small animal PET scanner. The distribution volume ratio (DVR) was measured for all subjects and group comparisons of D2/D3 binding among the cohort were made based on age and sex. Because two sequential studies were acquired from a single [F-18]fallypride batch, the effect of competing (unlabeled) ligand mass was also investigated. **Results:** Among this cohort, the rank order of regional D2/D3 receptor binding did not vary from previous studies with adult rhesus monkeys, with: putamen>caudate>ventral striatum>amygdala~substantia nigra>medial dorsal thalamus>lateral temporal cortex~frontal cortex. The DVR coefficient of variation ranged from 14%–26%, with the greatest variance seen in the head of the caudate. There were significant sex differences in [F-18]fallypride kinetics in the pituitary gland, but this was not observed for regions within the blood-brain barrier. Furthermore, no regions in the brain showed significant sex or age related differences in DVR within this small age range. Based on a wide range of injected fallypride mass across the cohort, significant competition effects could only be detected in the substantia nigra, thalamus, and frontal cortex, and were not evident above intersubject variability in all other regions. **Conclusion:** These data represent the first report of large cohort *in vivo* D2/D3 dopamine whole brain binding in the adolescent brain and will serve as a valuable comparison for understanding dopamine changes during this critical time of development and provide a framework for creating a dopaminergic biochemical atlas for the rhesus monkey.

Introduction

In recent years, *in vivo* identification of dopamine D2/D3 binding using PET imaging has focused on the extrastriatal regions of the brain, where the D2/D3 receptor density is reduced approximately 10-fold to 100-fold from the striatal regions of the putamen and caudate nucleus. The PET radioligands providing the most favorable imaging characteristics for visualizing the D2/D3 receptors in low density regions are the high affinity radiotracers [F-18]fallypride (Mukherjee et al., 1999) and [C-11]FLB 457 (Halldin et al., 1995). This pursuit of characterizing extrastriatal dopaminergic function is driven by clinical research in neuropsychiatric illness revealing disease specific differences, in diseases such as schizophrenia (Suhara et al., 2002; Talvik et al., 2003; Tuppurainen et al., 2003; Yasuno et al., 2004; Buchsbaum et al., 2006), Parkinson's Disease (Kaasinen et al., 2000, 2004), depression (Klimke et al., 1999) and Tourette Syndrome (Gilbert et al., 2006). There is also a strong interest in measuring dopamine transmission in the extrastriatal regions induced by either pharmacologic manipulation (Riccardi et al., 2006) or performance of a mental task (Aalto et al., 2005; Christian et al., 2006). These findings demonstrate the need for further research in the extrastriatal D2/D3 system and promote the use of animal models to further examine its potential role in behavior, neuropsychiatric pathology and targeted

* Corresponding author. Fax: +1 608 262 9440.
E-mail address: bchristian@wisc.edu (B.T. Christian).

1053-8119/$ – see front matter © 2008 Elsevier Inc. All rights reserved.
doi:10.1016/j.neuroimage.2008.10.020

drug development. The rhesus monkey (*Macaca mulatta*) serves as an excellent model for studying many of the neuroreceptor systems in the brain, including the dopaminergic system. Their anatomy, protein structure, receptor pharmacology and brain chemistry are considered to be similar to a large extent to humans. Neurodevelopmentally, the monkey brain mimics the human brain and many of the CNS tracts are found to be in close proximity in the monkeys and humans. Specific behaviors such as freezing, exploration and self-grooming have served as correlates to human emotional responses known to be related to the dopaminergic system (Pani et al., 2001). The rhesus animal model and PET imaging have also been used to unveil disruptions in the dopaminergic system as a result of moderate levels of fetal alcohol exposure (Roberts et al., 2004).

Neuroimaging of the extrastriatal D2/D3 receptors in the brain requires a high affinity radiotracer that is sufficiently cleared from nonspecific regions of the brain to provide a high target (specific) to background (nonspecific) binding ratio. [F-18]Fallypride possesses these attributes and has been validated in nonhuman primates (Christian et al., 2000 — rhesus; Slifstein et al., 2004 — baboons) and humans (Mukherjee et al., 2002; Siessmeier et al., 2005) to provide a quantitative index of D2/D3 binding. Further, the development of high resolution human and small animal PET imaging systems provides the necessary hardware to fully exploit the precise binding profile of [F-18]fallypride to the D2/D3 receptors throughout the brain. However, the use of high resolution imaging comes at the cost of requiring increased PET signal, i.e. a preserved number of counts per resolution element. A number of investigators have addressed the technical issues arising from small animal PET scanning and the tradeoff between higher resolution and reduced signal to noise ratio (SNR) and the implications on kinetic parameter estimation (Meikle et al., 2000; Sossi et al., 2005). Within the limits of a given scanner configuration, the improved PET signal can be achieved by increasing the amount of injected radiotracer, however, consideration must be given to minimize the competition of "tracer" ligand mass effects (Hume et al., 1998; Jagoda et al., 2004; Kung and Kung, 2005). Attention to mass effects of competing ligand is of particular concern for high affinity PET ligands, such as [F-18]fallypride and [C-11]FLB 457. For humans, it has been reported that doses of unlabeled FLB 457 should be less than 0.5 μg to avoid confounding occupancy of the drug (Olsson et al., 2004). For radiotracers with very low nonspecific uptake, such as [F-18]fallypride, the requirements for adequate PET signal are dictated to a large extent not by the target regions with elevated specific binding, but rather by the regions with low specific binding as well as the reference region. The large difference in rate constants of ligand binding ($k_{on}{\cdot}B_{max}$) and dissociation (k_{off}) of these radiotracers can require several hours of imaging to yield a stable measure of apparent binding potential (BP_{ND}). At these late time points the radiotracer concentration in the cortex and cerebellum is significantly reduced, presenting potential errors in accurately assaying the PET measured concentration. Due to these limits, the proper application of scanner related corrections such as scatter, randoms, attenuation and normalization are imperative to achieving accurate results (Bendriem and Townsend, 1998; Alexoff et al., 2003).

The purpose of this study is to provide a description of the distribution of the D2/D3 dopamine receptors in the adolescent brain of the rhesus monkey. As this is the first such report of large cohort results, a primary emphasis is placed on the methodological issues presented in using a high affinity D2/D3 radiotracer with small animal PET imaging. We focus on a close examination of the effects of ligand mass in our measurement of [F-18]fallypride binding. Also, the kinetics of [F-18]fallypride in the cerebellum are presented in detail to examine the potential effects of small but significant specific binding and low concentration measurement. These data are presented to provide the neuroimaging community with information regarding the expected variation in D2/D3 receptor binding in the rhesus monkey and also to provide baseline data for further large cohort comparisons based on longitudinal studies or drug development research.

Methods

NHP colony

A total of 33 *M. mulatta* (rhesus) underwent [F-18]fallypride PET scans for this work. The cohort has been described in detail in our previous work (Oakes et al., 2007; Kalin et al., 2008). It consisted of 23 female, 10 male; ages 3.2–5.3 years. Rhesus monkeys in captivity have a median life-span of 25 years (Colman and Kemnitz, 1999). Though translation to human years is nonlinear, we can approximate the equivalent age of this cohort to be 12 year old humans. All animals were pair-housed at the Harlow Primate Laboratory and the Wisconsin National Primate Research Center. Animal housing and experimental procedures were in accordance with institutional guidelines.

Radiotracer production

The [F-18]fallypride was produced according to previously reported methods using a modified chemistry processing computer unit (CPCU) (Mukherjee et al., 1995). The final product was formulated in a 5% ethanol saline solution for injection. To accommodate two PET imaging sessions per day, adequate batches of [F-18]fallypride were prepared from a single radiosynthesis. For the studies acquired as the second scan of the day (14 of 33 total studies), there was an average of 182 ± 11 min between the serial injections. The specific activity at the end of radiochemical synthesis was 2740 ± 1140 mCi/μmol, determined using analytic HPLC with UV absorbance detection. The PET scans were acquired with an injected amount of 5.0 ± 0.3 mCi of [F-18] fallypride and an injected mass of 1.8 ± 1.2 μg of fallypride.

High resolution small animal PET scanning

The monkeys were initially anesthetized with ketamine (15 mg/kg IM) and maintained on isoflurane (0.75%–1.5%) for the duration of the entire imaging session. The timing of anesthesia administration was closely monitored across the cohort, with a period of 33 ± 9 min between ketamine and radiotracer injection and 27 ± 10 min between isoflurane and injection. These will be referred to as ketamine timing and isoflurane timing for further analysis to investigate the possible effects of these drugs on radioligand binding (Nader and Czoty, 2008). The animals were also administered atropine sulfate (0.27 mg IM) to minimize secretions during the course of the experiment. The subject's head was positioned face downward in the prone position using a stereotaxic headholder to maintain consistent orientation for all the scanned monkeys. The animal was then placed in the P4 microPET scanner (Concorde Microsystems, Inc. Knoxville, TN). This high resolution PET has a reconstructed in-plane and axial spatial resolution of 2 mm full width half maximum with a volume resolution of approximately 8 mm^3. A 8.6 min transmission scan using a [Co-57] transmission point source was acquired to correct for the attenuation of the annihilation radiation within the tissue. The acquisition of the dynamic [F-18]fallypride PET scan was initiated with the injection of the [F-18]fallypride radiotracer. The dynamic data were acquired in list mode for a total of 150 min, to permit the calculation of quantitative results in all regions of the brain with dopamine D2/D3 receptors.

MRI scanning

Magnetic resonance imaging (MRI) data were acquired on all of the monkeys. Before undergoing MRI acquisition, the monkeys were anesthetized with intramuscular ketamine (15 mg/kg). Data were collected using a GE Signa 3 T scanner (GE Medical Systems, Milwaukee, Wisconsin) with a standard quadrature birdcage headcoil.

Subjects were positioned in a headholder for intersubject consistency. Whole brain anatomical images were acquired using an axial 3D T1-weighted inversion-recovery fast gradient echo sequence (TR=9.4 ms, TE 2.1 ms, FOV=14 cm, flip angle=10°, NEX=2, matrix=512×512, voxel size=.3 mm, 248 slices, slice thickness=1 mm, slice gap=0.05 mm, prep time=600, bandwidth=15.63, frequency=256, phase=224).

Data processing

Following the acquisition of the PET scan, the list mode data were binned into multiple time frames consisting of 5 frames of 2 min each followed by 14 frames of 10 min each. The data were then reconstructed using the vendor supplied software (microPET Manager version 2.3.3.6) by filtered back projection (with Fourier rebinning, 0.5 cm^{-1} ramp filter) to a voxel size of 1.26 mm×1.26 mm×1.21 mm and a matrix dimension of 128×128×63. All data were corrected for scanner normalization and dead time, scattered radiation (based on the direct calculation algorithm) and attenuation using segmented attenuation μ-maps.

Parametric images of distribution volume ratio (DVR) were generated for each animal based on the 150 min dynamic [F-18] fallypride scan utilizing the cerebellum as a reference region representing negligible specific binding. Time-activity curves from the cerebellum were generated by applying circular regions of interest over the outer lobes (predominately grey matter) on three separate transaxial slices (total sampling volume=1.11 cm^3) for each of the monkeys.

Parametric images were generated based on the multilinear arrangement of the functional equation described by others (Ichise et al., 1996; Logan et al., 1996), given as:

$$\int_0^T C(t)dt = \mathrm{DVR}\int_0^T C'(t)dt + \mathrm{DVR}/k_2' C'(T) - DVR/k_2 C(T) \quad (1)$$

where $C(t)$ and $C'(t)$ are the voxel and reference region concentrations (nCi/ml), respectively, k_2' is the reference region tissue to plasma efflux constant (min^{-1}), R_1 is the ratio of voxel to reference efflux constants (k_2/k_2') and DVR is the distribution volume ratio. This formulation was also used by Zhou et al. (2003) for radiotracers described by a single compartment model. For [F-18]fallypride kinetics, a two compartment model is necessary, requiring a period for linearization to be achieved. Thus, the regression parameters can be estimated for time $T>t^*$, when the terms become linear. A t^* of 45 min was used for these data based on previously measured estimates of k_2 and k_2' (41). The DVR serves as a metric of the apparent binding potential ($f_{ND}BP=BP_{ND}$), following the relationship:

$$\mathrm{DVR} = f_{ND}\mathrm{BP} + 1 \quad (2)$$

with f_{ND} representing the nondisplaceable (including free and nonspecifally bound) radiotracer fraction in the tissue space. We have chosen to use $\int_0^T C(t)dt$ as the dependent variable rather than an independent variable (as reported in Ichise et al., 2003) to increase the stability in the DVR estimation. The integration in the $\int_0^T C(t)dt$ serves to reduce the noise in the voxel-based data by temporal smoothing, however, it will also contribute to a biased estimation of the DVR regression coefficient, with greater noise levels resulting in an increasingly reduced DVR estimation (Carson 1993). To reduce noise at the voxel-based level, the images from each time frame were spatially smoothed using a 3×3 (in-plane) voxel median filter, similar to techniques proposed by Zhou et al. (2003). Though partially offsetting the high resolution of the small animal PET scanner, the median filter tends to preserve edges and furthermore this modest level of smoothing promotes the relative level of post-processing smoothness required for spatially normalized group comparison due to intersubject variations and random field theory (Worsley et al., 1992).

To facilitate group comparison of the DVR parametric images, the data were transformed into stereotaxically common space defined by the rhesus monkey atlas of Paxinos et al. (2000) using the FSL-Flirt software (Smith et al., 2004). To accomplish this, integrated images of [F-18]fallypride representing both radioligand delivery and binding were created using the entire dynamic study. These sum-images were then coregistered to the high resolution T1-weighted MRIs for each animal. The corresponding transformation matrix was then applied to the DVR parametric image to place both the PET and MRI data in common space. The T1-weighted MRI was spatially transformed to stereotaxic space using methods defined in our previous work (Kalin et al., 2005). This transformation for each animal was then applied to the PET DVR images to place all studies in common space. The image volumes were resliced into voxel dimensions of 0.625 mm isotropic. Regions of interest were defined on the MRI image of the template space for putamen (2.47 cm^3), caudate head (0.89 cm^3), ventral striatum — centrally placed within boundaries (0.14 cm^3), substantia nigra (0.27 cm^3), amygdala-basal region (0.15 cm^3), midline region of inferior thalamus (0.15 cm^3), frontal–dorsal prefrontal cortex (0.94 cm^3), anterior cingulate cortex (1.78 cm^3), temporal–superior temporal sulcus (1.22 cm^3) and pituitary (0.05 cm^3). These areas were selected based upon a relative uniformity of [F-18]fallypride binding within each region and minimal overlap with surrounding structures that could contribute to a spillover of radioactive signal. For example, the basal amygdala was defined as the inferior portion of the total amygdala region and was chosen as a separate region based on the high focal D2/D3 binding and clear separation from the inferior putamen.

To examine the potential of variability being introduced into the dataset due to the MRI coregistration and spatial normalization procedures, we also obtained region of interest DVR values from the PET data in native space. The regions of the putamen and substantia nigra were selected based on their distinctive pattern of [F-18] fallypride binding and the frontal cortex was chosen as the region outside the basal ganglia. Circular ROIs of fixed volume were centrally applied to the peak regions of the putamen (0.46 cm^3 — spanning 5 image planes), substantia nigra (0.08 cm^3 — 3 image planes) and frontal cortex (0.40 cm^3 — 3 image planes). It is important to distinguish that these ROIs were drawn over the regions of peak concentration on the PET images (i.e. based on chemoarchitecture) in contrast to the template ROIs which were traced on the MRI template defined with reference to Paxinos et al. (2000). No corrections were applied to account for resolution effects (i.e. partial volume effects). Although such corrections are important for individual quantitative measures, for groupwise statistical analysis the advantage is minimal, in part because the correction is undone during the spatial smoothing step.

Data analysis

The DVR values for the region of interest data were compared across the entire cohort to investigate the variability in [F-18] fallypride D2/D3 binding. Group-based sex differences were investigated using a two-sample t-test. Hierarchical multiple regression analysis was performed to examine the effects of the experimental variables on [F-18]fallypride DVR. Because a single batch of radiopharmaceutical was used for two sequential PET scans for some of the experiments, we closely examined the effects of injected ligand (unlabeled fallypride) mass on the measurement of DVR. A correlation analysis of DVR with the injected fallypride mass was performed across the entire cohort for each ROI. Based on the equilibrium relationship between the bound (B) and free (F) ligand, the fractional occupancy (B/B_{max}) of the ligand for the receptor site is given by:

$$\frac{B}{B_{max}} = \frac{F}{K_D + F} \quad (3)$$

thus being dependent only on the free ligand concentration (F) and the equilibrium dissociation rate constant (K_D) and independent of the

local receptor concentration B_{max}. Though true equilibrium is not sustained (or necessarily achieved) for bolus injection studies, this relationship indicates that the measured DVR should be reduced for the studies with increased injected mass (or decreased specific activity), e.g. for the second injection during a multiple-subject PET imaging session. These effects of competing ligand mass (unlabeled fallypride) were examined by comparing the measured DVR with two indices: i) the injected mass scaled to body weight (μg/kg) and ii) the integrated cerebellar time-activity curve (AUC). The PET measured cerebellar AUC represents the nondisplaceable (free and nonspecifically bound) ligand that crosses the blood brain barrier (BBB), which is a more accurate measure of "free" ligand than the injected mass (scaled to body weight) index of μg/kg as is used in non-imaging pharmacological studies. The AUC index minimizes the cohort variability caused by peripheral metabolism of ligand by excluding the measurement of polar metabolites that do not cross the BBB. Though the AUC does contain a component of nonspecifally bound ligand, and perhaps small amounts of specifically bound ligand, we must assume the variability in this component is minimal as it is also present in the outcome measure of DVR. The AUC was calculated by integrating the decay corrected cerebellar data over the entire 150 min of PET acquisition, with units of radioactivity (AUC_r) and also by converting to units of pmol/mL·min (AUC_c) by division with the [F-18] fallypride specific activity. Simulations are presented to illustrate the theoretical effects of ligand mass on the measured DVR (see Fig. 5). These simulations were performed using previously reported *in vivo* parameters for [F-18]fallypride (Christian et al., 2004) and the AUC_c values were scaled to match the nondisplaceable concentration of the tissue at the time of equilibrium based on simulated data.

Results

Cerebellum kinetics

The time course of [F-18]fallypride in the region of the cerebellum is shown in Fig. 1 for the decay corrected data. These data reveal high initial uptake of radiotracer followed by relatively rapid clearance with only approximately 0.003% injected dose (I.D.) per cc of tissue at 2 h post-injection. These data were fit to a bi-exponential curve to provide an estimate of the clearance of radiotracer from the cerebellum, with the results given in Table 1.

The figure reveals relatively close agreement in kinetics across the cohort with the mean cerebellar concentration during the final 30 min revealing a coefficient of variation of 27% (0.0027±0.0007% I.D./cc)

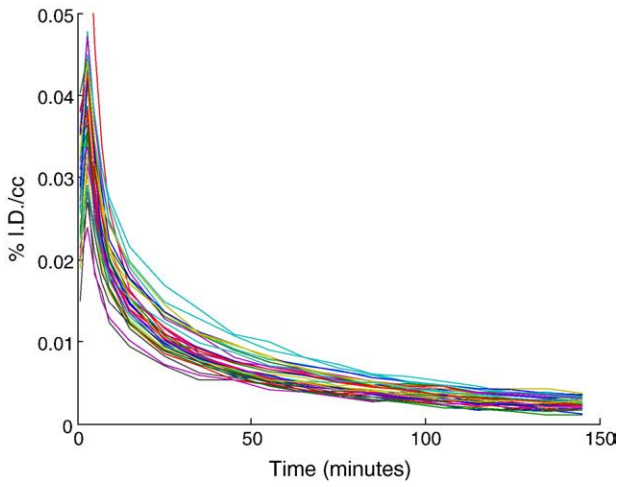

Fig. 1. Cerebellum time-activity curves for [F-18]fallypride normalized to percent injected dose (% I.D.) per cc of tissue.

Table 1
[F-18]Fallypride kinetics in the cerebellum

Cerebellum: $\%I.D. = a_1 e^{-\lambda_1 t} + a_2 e^{-\lambda_2 t}$			
a_1	λ_1	a_2	λ_2
0.031±0.016	0.131±0.051	0.013±0.004	0.012±0.003

Decay corrected data fit following the peak activity, at times of 6–150 min. For all studies the peak concentration occurred during the second time frame (2–4 min) with the scan initiated with a 30 s bolus infusion of radiotracer.

and all values within 2 standard deviations of the mean. There was also no significant correlation between cerebellar AUC_r and animal weight ($r=-0.18$, $p<0.31$).

Regional D2/D3 dopamine binding

Fig. 2 highlights the extrastriatal regions of the brain demonstrating high focal binding of [F-18]fallypride. Shown in Fig. 3 are PET time-activity curves of [F-18]fallypride in the various regions of the brain. The DVR values for the regions of interest across the entire cohort are shown in Table 2, with the exclusion of 2 animals having DVR values that were more than 2 standard deviations from the group mean. These data illustrate the range in specific D2/D3 binding for regions of high, medium and low D2/D3 receptor density. The coefficient of variation (s.d./mean*100%) for these regions is shown for both DVR and BP_{ND} (=DVR−1). The thalamus has a highly heterogeneous distribution of D2/D3 receptors throughout the subregions. The thalamic ROI was centered over the midline region of the inferior thalamus, revealing the highest uptake of the thalamic subregions. The rank order of D2/D3 binding for each animal was approximately consistent across all regions, i.e. the monkeys with the highest putamen binding also had the highest binding in the amygdala, substantia nigra, anterior cingulate, etc. The Spearman correlation coefficient for DVR between the regions was highest among the striatal regions with $0.90>\rho>0.65$ between the putamen, caudate and ventral striatum. For the other regions, the correlations between regions ranged from 0.20–0.60 and were positive in all cases. The pituitary revealed no correlations outside the range of $-0.10<r<0.10$, though it must be noted that some of the assumptions of the reference region model fail in this region outside the blood brain barrier.

DVR measurements were also made on the native PET images, prior to spatial processing, to minimize potential intersubject variance due to spatial coregistration and normalization. ROIs were drawn only for the putamen, substantia nigra and frontal cortex based on the PET images. The DVRs for these ROIs were significantly greater compared to the template based values (shown in the Table 2) due to the central ROI placement on the PET data, however, there was a slightly reduced coefficient of variation for each region: putamen (mean=28.6, COV=19%, COV BP_{ND}=20%), substantia nigra (3.40, 13%, 18%) and frontal cortex (1.52, 12%, 35%), suggesting that a small but measurable amount of variance is introduced due to the process of spatial normalization with MRI-based ROIs, or that these structures are not homogenous with respect to dopamine response, and/or that a partial volume correction might be needed. There was also a very strong correlation between the native PET and template based DVR values, $r=0.98$, 0.92, 0.92 for the putamen, substantia nigra and frontal cortex, respectively.

The effects of the experimental variables, including sex, age, weight, and timing of anesthesia (ketamine and isoflurane) administration on D2/D3 binding using hierarchical multiple regression are shown in Table 3. Based on the Welch two sample *t*-test, there was no significant sex-based difference in age ($p=0.31$), weight ($p=0.11$), ketamine timing ($p=0.15$), isoflurane timing (0.23), fallypride mass (=0.89) or AUC_c ($p=0.43$). Also, there was no significant correlation between age, weight, ketamine timing, isoflurane timing and fallypride mass (μg/kg) explanatory parameters. Though all of the brain

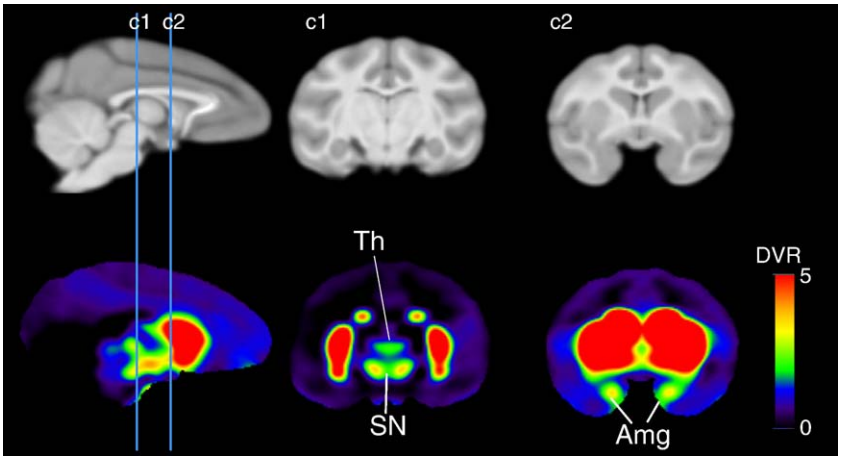

Fig. 2. Extrastriatal regions with high focal uptake of [F-18]fallypride. Coregistered MRIs (top row) reveal two corresponding coronal slices (indicated by c1 and c2 on sagital view) and regions of elevated [F-18]fallypride binding (bottom row) in the thalamus (Th), substantia nigra (SN) and amygdala (Amg) in addition to the striatum which is set to a threshold of red.

regions displayed higher average [F-18]fallypride binding in the females, the only region revealing a significant difference based on sex was the pituitary, with the females displaying 38% greater uptake. Further analysis considerations in the pituitary will be addressed in the Discussion. Within the brain, there were no significant differences (when corrected for multiple comparisons) in [F-18]fallypride binding due to age or weight when controlled for sex. As seen in the table the range in age (3.20–5.26 yr) and weight (4.6–8.7 kg) of the subjects was relatively small. Shown in Fig. 4 are the DVR values in the putamen and amygdala plotted as a function of age.

Fallypride mass effects

Table 3 also gives the results for the correlation of [F-18]fallypride binding with the body mass scaled fallypride and total integrated nondisplaceable fallypride (AUC_c). It can be seen that a statistically significant relationship with AUC_c was measured in the substantia nigra, thalamus, and frontal cortex, with only the thalamus showing significance when corrected for multiple comparisons. The individual data points for four of the regions are shown in Fig. 5, using the native PET ROIs. Also plotted is the theoretical relationship between the measured binding (DVR-1) and the total integrated nondisplaceable fallypride (AUC_c). This curve is included only to serve as an indicator of the theoretical mass dependent effects on DVR for constant values of B_{max} and K_D, which cannot be assumed for these data due to intersubject variability.

Discussion

Normative databases of PET neuroligand binding have been reported in humans for dopamine synthesis, D_1 receptors, D_2 receptors, and transporters (Ito et al., 2008) and 5-HT_{1A} receptors (Rabiner et al., 2002; Costes et al., 2005). These provide an important resource to the neuroimaging community not only for exploring specific regional variations in neuroreceptors but also for providing insight into sample size considerations and experimental methodologies. As molecular imaging techniques such as small animal PET expand in scope for studying disease, treatment response and

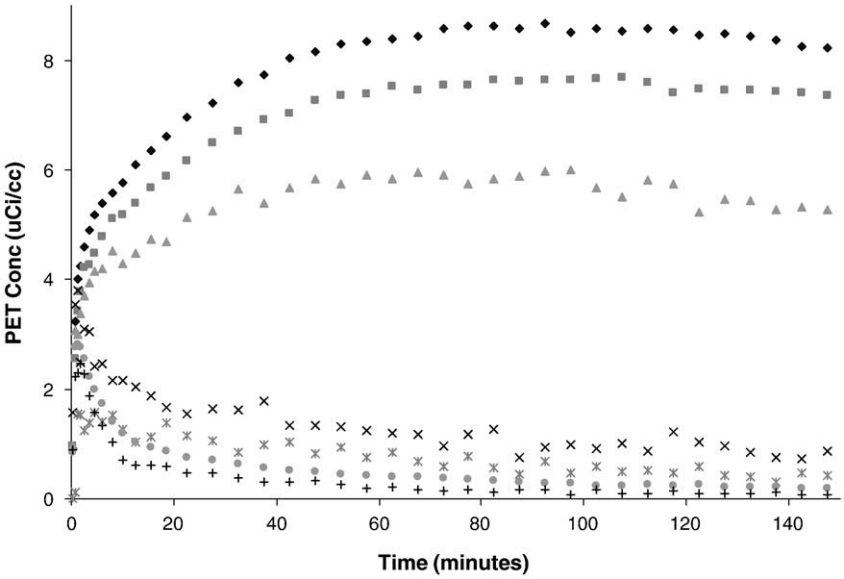

Fig. 3. PET time-activity curves of [F-18]fallypride in the regions of the brain with varying D2/D3 receptor density. Shown in order of highest to lowest uptake are putamen (♦), head of caudate (■), ventral striatum (▲), pituitary (x), amygdala (✱), frontal cortex (●) and cerebellum (+). The time course of the thalamus and substantia nigra (not shown) are similar to the amygdala and the temporal cortex (not shown) closely resembles the frontal cortex.

Table 2
Cohort distribution volume ratio (DVR) of [F-18]fallypride

	Mean DVR	Standard deviation	%COV (COV BP_{ND})
Putamen	21.1	4.5	21% (22%)
Caudate head	16.8	4.4	26% (28%)
Ventral striatum	12.1	2.0	17% (18%)
Pituitary[a]	2.75	0.91	33% (52%)
Amygdala	2.63	0.64	24% (39%)
Substantia nigra	2.49	0.35	14% (23%)
Thalamus	2.13	0.40	19% (35%)
Anterior cingulate	1.74	0.24	14% (32%)
Frontal cortex	1.47	0.23	16% (49%)
Temporal cortex	1.42	0.28	19% (67%)
Cerebellum	1.00[b]	–	–

[a] Pituitary — the reference region model has not been validated for the pituitary. These values are target/cerebellum ratios.
[b] Cerebellum — DVR = 1.00 by definition.

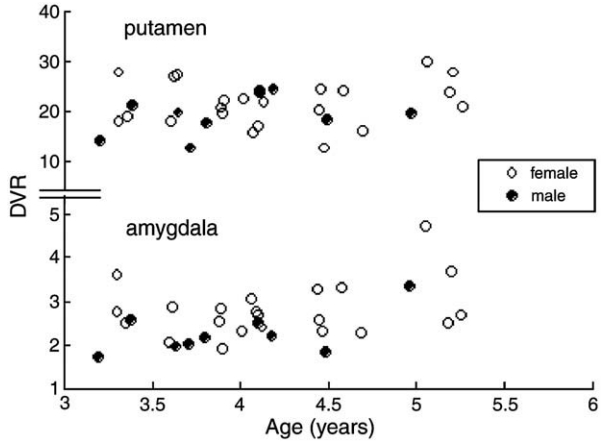

Fig. 4. DVR as a function of age in the regions of the putamen and amygdala for both females and males.

screening new candidate drugs for therapy (Lee and Farde, 2006; Strome and Doudet, 2007), it is necessary to fully scrutinize the methodological and experimental parameters to characterize sources of experimental and biological variance. The rhesus monkey provides an excellent model for studying neurochemical alterations in the brain implicated in neuropsychiatric illness. The neurochemical pathways and behavioral similarities with humans, particularly for the dopaminergic and serotonergic systems, allow the investigator to exploit the wide array of developed PET tracers targeting the various receptor subtypes.

The large cohort of rhesus monkeys in the current study permits reliable baseline measurements of D2/D3 binding in both the striatal and extrastriatal regions of the brain, and enables investigation of regional binding and variability of [F-18]fallypride in the rhesus monkey using small animal PET imaging. During the acquisition of the scans, these animals were in the adolescent period of development. At present we cannot provide a comparison of D2/D3 binding with other age groups acquired with high resolution small animal PET systems, thus it is not possible to explore characteristics of D2/D3 dopaminergic innervation unique to this stage of development. However, this dataset will provide a valuable resource for future comparisons of age dependent changes in D2/D3 receptors. In this section we provide an overview of the regional distribution of D2/D3 receptors from this large cohort. Further, to explore potential sources of variability beyond biological differences we examine the effects of competing unlabeled ligand mass, an issue which continually arises for detecting nanomolar levels of receptors in the brain.

Distribution of D2/D3 receptors in the rhesus brain

The general patterns of [F-18]fallypride binding in the rhesus brain are similar to previous reports of D2/D3 binding in humans (Kessler et al., 1993; Olsson et al., 1999; Mukherjee et al., 2002), though there are some differences in the rank order of the brain regions (discussed below). Because these data were analyzed in standardized space, the reconstructed images were not corrected for partial volume effects. Thus we do not make an attempt to quantitatively compare D2/D3 binding between regions. However, regional DVRs in the putamen, substantia nigra and frontal cortex revealed very high correlations (98%, 92%, 92%, respectively) between native and standardized space

Table 3
Effects of DVR with experimental variables

t-test			Multiple regression with DVR					
	Sex		Age	Weight	Ketamine timing[a]	Isoflurane timing[a]	Injected fallypride	Free fallypride AUC_c
Mean (SD)	F — 23 M — 10		4.09 yr (±0.60)	5.82 kg (±1.08)	33 min (±9)	27 min (±9)	0.31 μg/kg (±0.21)	53 pmol/mL9min (±35)
	DVR	*p*-value	*p*-values					
Putamen	21.8±4.4 19.0±4.2	0.26	0.22	0.41	0.57	0.53	0.98	0.65
Caudate head	17.5±4.2 14.8±4.8	0.32	0.04	0.39	0.52	0.46	0.85	0.58
V. stri.	12.4±2.1 11.4±2.0	0.36	0.27	0.41	0.26	0.31	0.31	0.31
Pituitary	3.03±0.86 1.89±0.23	**0.003**	0.07	0.37	0.16	0.16	0.53	0.18
Amygdala	2.67±0.42 2.35±0.38	0.07	0.02	0.41	0.56	0.45	0.14	0.18
S.N.	2.55±0.33 2.33±0.38	0.15	0.08	0.57	0.05	0.05	0.05	0.03
Thalamus	2.13±0.39 2.13±0.47	0.92	0.42	0.75	0.01	0.01	**0.001**	**0.0004**
Ant. cing.	1.76±0.24 1.68±0.21	0.52	0.21	0.42	0.63	0.51	0.57	0.47
Frontal	1.49±0.28 1.24±0.13	0.30	0.72	0.09	0.61	0.50	0.11	0.027
Temporal	1.46±0.29 1.31±0.23	0.26	0.18	0.09	0.70	0.95	0.26	0.06

Bold — significant when corrected for multiple comparisons.
[a] Ketamine (and isoflurane) timing is the time period between ketamine (isoflurane) administration and the injection of radioligand.

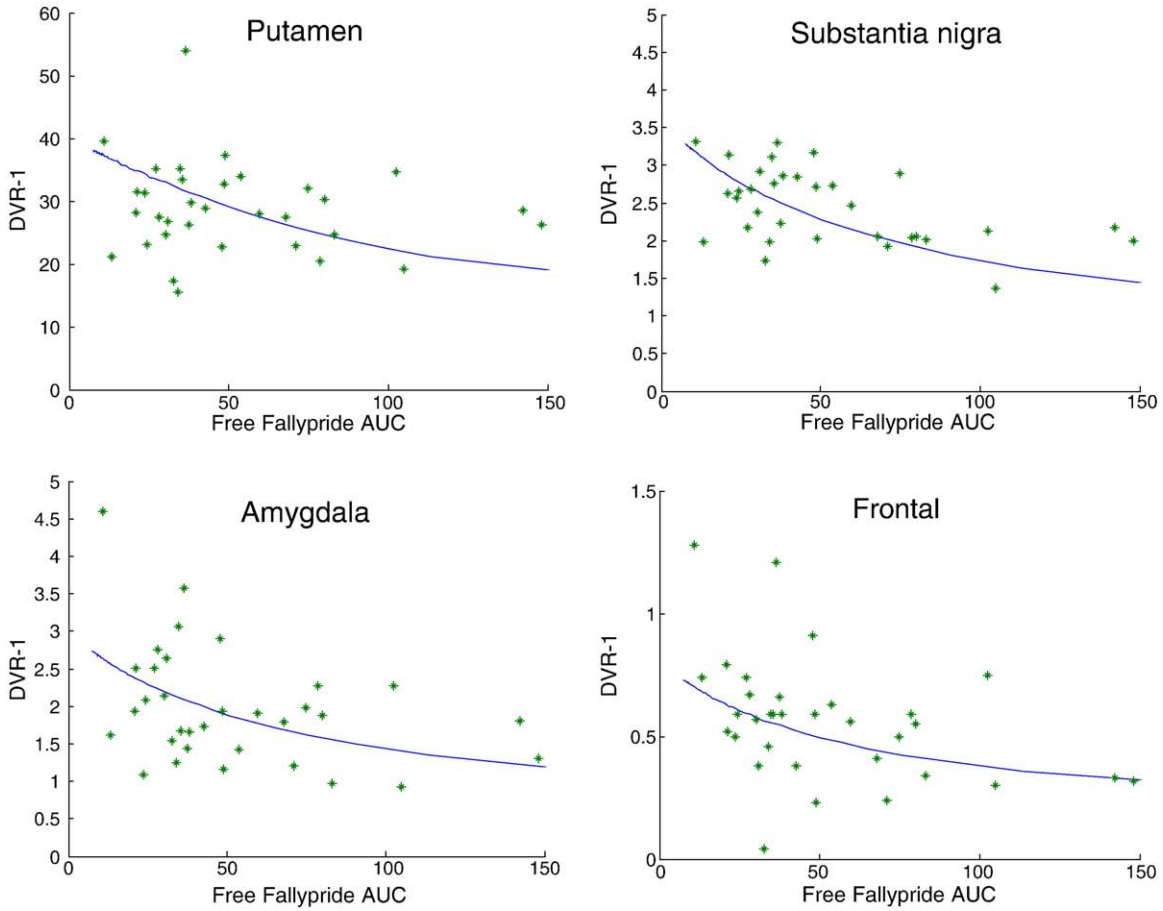

Fig. 5. [F-18]Fallypride binding as a function of the integrated free fallypride across the entire cohort. The free fallypride represents the integrated concentration of fallypride (AUC_c) in the region of the cerebellum divided by the specific activity. DVR−1 represents the bound to free ratio of the [F-18]fallypride binding. The solid line (−−) represents the relationship between the bound to free ratio (DVR-1) and the free ligand based on simulation data. This curve is valid for a constant receptor density (B_{max}) and affinity ($1/K_D$) and served as an indicator of the expected decrease in DVR-1 as a function of increased mass. Only the plot of the substantia nigra reveals a statistically significant relationship between DVR-1 and AUC_C.

data suggesting they are relatively homogenous across subjects, which implies that a partial volume correction would cause a similar change across subjects within a particular structure. The highest concentration of dopamine D2/D3 receptor binding was measured in the striatal regions of the brain with the largest DVR values found in the putamen and the head of the caudate (see Table 2), with no noticeable variation in the binding of [F-18]fallypride within these clearly visualized regions. The regions of the ventral striatum and body of the caudate (not shown in Table 2) displayed DVR measurements of approximately 50% reduction compared to values in the putamen. Outside of the striatum, the regions of the substantia nigra, thalamus and amygdala all displayed approximately the same magnitude of DVR, which is roughly tenfold less than the putamen. In the thalamus, there are only two regions demonstrating focal uptake of [F-18]fallypride. The most extensive thalamic uptake is seen in the midline region of the inferior thalamus, with lower but significant binding seen in the region of the anterior medial nuclei. The limited resolution of the small animal PET scanner and the smoothing effects of spatial normalization process leave some uncertainty in the precise labeling of thalamic subregions, with our regions likely including a portion of the neighboring superior colliculi.

The rhesus thalamic pattern of D2/D3 binding is noticeably different than reported in humans as detailed by Rieck et al. (2004) using autoradiographic sections, where the highest levels of binding are seen in the midline anterior regions and significantly lower binding in the region of the medial dorsal nucleus. Fig. 6 provides a comparison of human and rhesus [F-18]fallypride binding to visually illustrate the difference in regional thalamic binding. Identification of binding in specific thalamic nuclei of the rhesus monkey for comparison with humans will require *in vitro* labeling with autoradiography, but such data is not available at this time for the rhesus monkey. Species related comparative analysis will be of great interest in nonhuman primate models of neuropsychiatric disease, such as substance abuse (Porrino et al., 2004; Nader and Czoty 2008), parkinson's disease (Emborg 2007) and schizophrenia (Lipska and Weinberger, 2003), where thalamic dopaminergic innervation may be compromised.

The cortical areas (frontal and temporal) displayed low but significant amounts of specifically bound receptor, with approximately 30% of the measured PET signal originating from bound radiotracer. In humans, there is significantly greater binding in the temporal gyri (medial and inferior) compared to other cortical regions in the brain. In our previous work with [F-18]fallypride in humans, we found 3–4 times greater BP_{ND} in the temporal region compared to the frontal cortical regions (Mukherjee et al., 2002). In baboons using [C-11]FLB457, Delforge et al. (1999) reported a 6-fold increase in temporal cortex B_{max} compared to the frontal cortex, though it is unclear if this work included regions of the parahippocampal cortex and amygdala with elevated D2/D3 binding. Our previous findings in rhesus monkeys using a high resolution human brain scanner are in agreement with our present study revealing approximately uniform levels of D2/D3 binding in the frontal and lateral temporal cortices

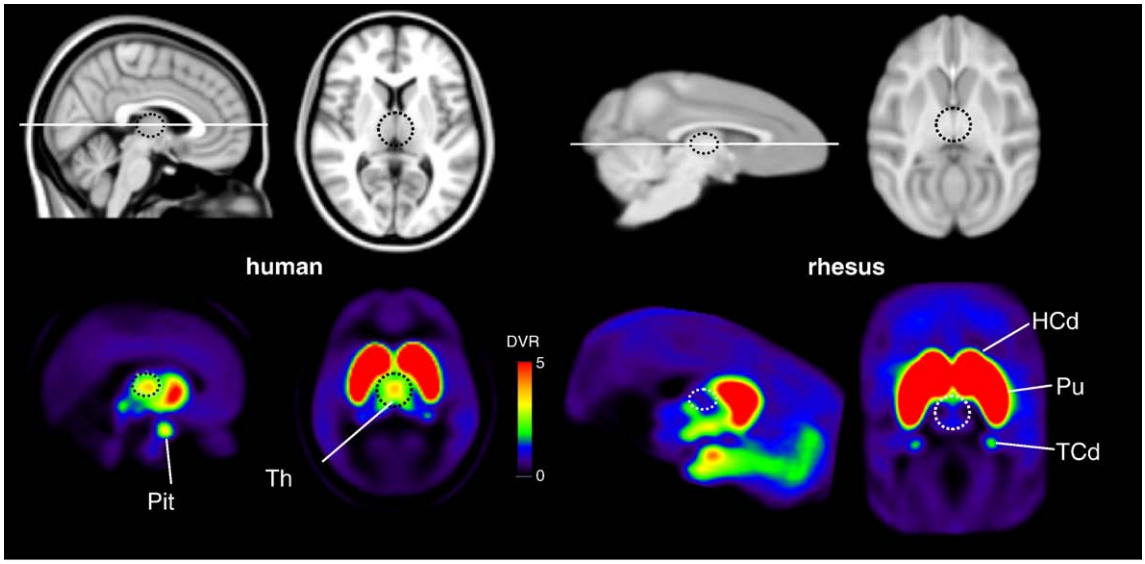

Fig. 6. Thalamic [F-18]fallypride binding in the human and the rhesus monkey. The human DVR [F-18]fallypride images (taken from normal controls: $n=15$, Buchsbaum et al., 2006) were spatially normalized to the MNI152 MRI datset (top left) (Lancaster et al., 2007). The transaxial slice goes through the mid-thalamic region (outlined for reference), 8 mm above the AC–PC plane. The rhesus DVR [F-18]fallypride images were spatially normalized to the rhesus standardized space (McLaren et al., in press) (top right, skull stripped). The transaxial slice is 6 mm above the AC–PC plane. Unlike humans, the rhesus monkeys display low binding in the anteroventral region of the thalamus. The thalamic regions (Th) on the transaxial slices do not outline the full extent of the thalamic nuclei. Other labeled regions include the pituitary (Pit), caudate head (HCd), caudate tail (TCd) and putamen (Pu).

(Christian et al., 2000; Christian et al., 2004), enforcing the finding that there is a mismatch between humans and rhesus monkeys in temporal cortical binding.

The coefficient of variation in DVR (see Table 2) across the cohort was consistent over all regions with the exception of the pituitary, ranging from 14%–26%, with the largest COV seen in the caudate head. However, if we consider COV in BP_{ND} (=DVR−1), which is of greater interest for testing group differences in B_{max}, a larger variation is seen in the low D2/D3 receptor density regions, particularly the cortical areas. In the striatum, this variation is close to that reported with [C-11] raclopride of 22–26% reported in the literature in humans (Farde et al., 1995). Also, the variation in subcortical regions are in line with COVs reported in humans of approximately 30% for PET D2/D3 binding (Olsson et al., 1999; Asselin et al., 2007). These data can be used as guidance for power analysis for future experiments. For example, to detect a 20% change in DVR in the amygdala between groups, a sample size of approximately 24 monkeys is needed for 80% power and $p<0.05$.

The only significant correlation of [F-18]fallypride binding with sex, age and weight variables was a sex based difference in the pituitary (Table 3). We have previously reported significant specific binding in this region (Mukherjee et al., 2002), following earlier reports using *in vitro* binding assays with [I-131]epidipride (Kessler et al., 1993). It is important to note the limitations of a reference region method of analysis for determining pituitary binding. The reference region provides the time course of the nondisplaceable ligand contained within the blood-brain barrier (BBB). However, the pituitary lies outside this protective barrier so we can no longer make the assumption that the nondisplaceable space distribution volume (K_1/k_2) is equivalent with the reference region (cerebellum). Similarly we can assume that a portion of the signal in the pituitary represents blood-born hydrophilic metabolites, which represent approximately half of the plasma concentration at 60 min post-injection. Thus there is the possibility that a component of the differences between sexes is due to peripheral metabolism of [F-18]fallypride. For these reasons, we report a pituitary to cerebellum ratio, rather than DVR. For this cohort we found ratios of 3.03±0.86 for females and 1.88±0.23 for males ($p<0.0009$). In female rats, it has been shown that D2 receptor expression and dopamine itself displays changing levels during estrous cycle, pregnancy and lactation (Zabavnik et al., 1993). None of the females in this cohort were pregnant during the experiment and there was no attempt to control for the period of the estrous cycle and the scan date. Observations of the onset of mensus were recorded (based on sex skin color and swelling), however, this information was not included in the analysis. There was no significant sex difference in %COV DVR in any other regions of the brain, thus despite an unbalanced cohort (23 females, 10 males) there is no suggestion that increased variance could be attributed to sex differences, which is consistent to previous studies in the cynomolgus monkey focusing on the striatal region (Nader and Czoty 2008 — for review).

Methodological considerations

Reference region kinetics

The kinetics of [F-18]fallypride in the cerebellum were closely examined because the estimation of DVR is heavily dependent on the time course of [F-18]fallypride in this region. The cerebellum serves as a reference region exhibiting negligible D2/D3 binding for all commonly used substituted benzamides, including [C-11]raclopride and [C-11]FLB357. The presence of small yet significant D2 receptor-specific binding in the cerebellum has been reported frequently (Delforge et al., 1999; Olsson et al., 1999, 2004) and associated bias in the measured DVR has been well characterized in humans for FLB457 (Asselin et al., 2007). The effect of specific cerebellar binding on the estimation of target region binding is given by the relationship: $DVR_{apparent}=DVR_{true}/(DV_T/DV_{ND})$, for the total (T) and nondisplaceable (ND) cerebellar distribution volume (DV). For these data, if we assume a specific binding in the cerebellum that is 75% less than the frontal cortex, as reported by Olsson et al. (1999) for FLB457, the estimates of [F-18]fallypride reported herein would be underestimated by 11% (i.e. $DV_T/DV_{ND}=1.11$). Analysis based on the measurement of the arterial input function would remove potential bias due to specific binding in the reference region, however, the task of gathering and analyzing arterial input measurements present their own challenges and uncertainties, thus the potential of introducing bias in the DVR or BP_{ND} measurements is a commonly accepted tradeoff for the experimental ease of using reference region methods. We are not aware of any reports on the density of D2/D3 receptors in the cerebellar lobes of the rhesus monkeys, however, based on human PET

data with [C-11]FLB457 reporting a BP=0.17 (n=8) (Olsson et al., 1999) we can estimate that the variation due to reference region specific binding will be less than 5% for this dataset.

The relatively low levels of nonspecific binding observed with highly selective, high affinity D2/D3 radiotracers such as [F-18] fallypride or [C-11]FLB457 permit measurement of extrastriatal regions in the brain. However, the low levels of radioligand signal in the reference regions present a challenge for the accurate quantitative measurement of DVR due to reduced noise equivalent count rates, requiring strict attention to the implementation of scanner normalization and scatter correction.

Prior to the initiation of this protocol we performed a phantom study with a NEMA cylindrical phantom and simulated [F-18] fallypride distribution to examine the accuracy of radioactivity recovery within the context of our experimental design. These data revealed the error in the measurement of radioactive concentration ([true-measured]/true) was less than 2% at 100 nCi/cc, with the error increasing to 15% at 50 nCi/cc and rapidly increasing with lower concentrations, using ROIs equivalent to the cerebellar regions. Based on our previous experience with fallypride in the rhesus monkey, a 5 mCi injection was chosen to target a cerebellar concentration in excess of 50 nCi/cc at 2 h post-injection. The mean measured concentration in the cerebellum for these studies with 5 mCi injection was approximately 75 nCi/cc at 2 h post-injection (without decay correction). Only 4 studies were below this target concentration, with the lowest at approximately 40 nCi/cc.

There was no significant correlation between cerebellar radioactivity AUC_r (nCi/cc·min) and animal weight with a range in weight of 3.4–8.7 kg (5.8±1.1 kg). The AUC_r represents the total amount of free (and nonspecifically bound) radioligand presented to the tissue and it would be expected that dilution in a larger (blood) volume would result in a reduced AUC_r based on the frequently used approximation that the total blood volume is roughly 10% of body weight (Fox et al., 2002). Though this is considered an imprecise estimate, a statistically significant correlation was expected between animal weight and cerebellar AUC_r as supported by radiotracer studies of allometry (Lambrecht and Eckelman, 1983). This lack of correlation may be due to biological variation in components of the nondisplaceable space distribution volume, which relates the reference (C_{ref}) and plasma concentration (C_a) according to: $f_P C_a = f_{ND} C_{ref}$, where f_P and f_{ND} are the free fractions in the plasma and reference compartment, respectively. Other potential explanations could be the peripheral metabolism of [F-18]fallypride into hydrophilic species which are unable to cross the blood-brain barrier in the cerebellum as well as physiological factors resulting in degradation of the radioligand (Jagoda et al., 2004). To compare this to the variation in cerebellar kinetics with human data, we re-examined our earlier work comparing subjects with schizophrenia with matched controls (Buchsbaum et al., 2006). Based on 15 normal human controls, there was also a lack of correlation between cerebellar radioactive AUC_r and subject weight (ρ=−0.02, p<0.95). The coefficient of variation in the human cerebellar AUC_r was 18%, compared to 19% for this cohort of monkeys. Though there is limited information comparing [F-18]fallypride kinetics in humans and rhesus monkeys, this close agreement between cerebellar AUC_r despite dramatically different PET scanner configurations between the two species supports the notion that the variation in cerebellar AUC is not due to potential systematic errors in the measurement of low level radioactivity but rather due to biological variability.

Mass effects

For this work, we chose to perform two sequential studies (i.e. injections) from a single batch of [F-18]fallypride to ease the demands for radiopharmaceutical production. Because radioligand imaging studies suffer from poor count based information density, it is important to preserve count statistics across subjects, leading to our choice to inject similar amounts of [F-18] radioactivity for all studies (5 mCi) rather than similar fallypride ligand mass. If the goal had been equal mass injections, the 182±11 period between the injection of the first animal and the second animal would translate into a 70% reduction in [F-18]fallypride radioligand. Such a discrepancy in counting statistics have the potential to introduce biased estimates of DVR calculations, particularly for voxel based analysis (Ichise et al., 2002). However, the 3-fold increase in fallypride mass between injections accompanying constant radioactivity injections warrants close examination for potential confounds due to the presence of additional competing ligand.

The relationship between the concentration of receptor-bound and free ligand is well established based on *in vitro* methods. These concepts can be extended to *in vivo* settings utilizing the ability of PET to assay the concentration of the radioligand. Using the methods presented by Holden et al. (2002), an *in vivo* binding relationship can be defined as:

$$\frac{B}{F} = \mathrm{BP} \cdot K_D^{app} / \left(K_D^{app} + F\right), \tag{4}$$

where B/F represents the bound to free concentration of ligand (fallypride) and BP is the binding potential $\left(=B_{max}/K_D^{app}\right)$. This relationship was plotted in Fig. 5 to illustrate the theoretical changes that would be expected in B/F(=DVR−1) as a function of increasing free ligand. There are several issues with applying this equation to the data in Fig. 5 that requires further explanation. First, the relation of B/F vs. F applies only for constant B_{max} and K_D^{app}, i.e. as would be expected from a single subject for a series of injections. For the theoretical curves (in Fig. 5) the B_{max} and K_D^{app} were held constant to values reported in our earlier work (Christian et al., 2004) and were not taken from this cohort. Second, the x-axis in this figure serves only as an index of the free (F) ligand concentration representing all nondisplaceable ligand and does not account for potential variability in the fraction which is not nonspecifically bound (f_{ND}). It should also be noted that the x-axis from Fig. 5 plots the free fallypride AUC_c which serves as an index of the free (F) concentration.

Based upon the simulations in Fig. 5, we can estimate a 23% difference in ligand occupancy (or BP_{ND}) between the monkeys in the lower- and upper-half mass groups (approximated as the first and second scanning groups of a session) if a constant K_D is assumed. Significant (uncorrected for multiple comparisons) correlations between DVR and fallypride mass were only observed in the substantia nigra, thalamus, and frontal cortex. This provides an indication of the intersubject variability in the various regions of the brain that were examined, which was lowest in these regions. The inability to significantly measure this difference in other brain regions indicates it is a comparatively small source of variance with respect to the intersubject variability. By making the assumptions that K_D^{app} is constant across all subjects (~0.4 nM) and that the free concentration is similarly proportional to the injected mass, it can be estimated that the coefficient of variation (COV) in DVR due to ligand mass effects alone would be approximately 15% for these data. Thus, differences in specific activity have the potential to serve as a significant source of variability, given the variance from the different sources propagates in quadrature for normal distributions. Though the injected ligand mass can be assigned as a covariate in group comparisons, unfortunately it is not possible to apply an analytic correction to the measured DVR to account for the competing ligand because of the intrinsic correlation in B_{max} and K_D^{app} in the estimation of DVR, neither of which are known nor assumed to be constant. An alternative to account for the effects of variable ligand mass and to uncouple B_{max} and K_D^{app} parameters is to perform multiple injection studies of radioligand, with separate injections of varying ratios of radiolabeled and unlabeled ligand (i.e. specific activity). These methods serve as the gold standard for isolating potential disease specific alterations in receptor density and receptor–ligand affinity, however, at the cost of significantly increased

experimental complexity as well as increased intersubject variability in the independent B_{max} and K_D^{app} parameters (Logan et al., 1997).

For human PET studies, regulatory restrictions generally limit the injectable mass to avoid pharmacological doses (e.g. <5% receptor occupancy), with higher levels permitted in nonhuman primates. Though significant radioligand occupancy holds the potential to induce pharmacological effects via mechanisms such as receptor trafficking or changing levels of endogenous neurotransmitter, there is no evidence based on previous experiments with D2/D3 antagonists PET radioligands that the D2/D3 receptor system becomes altered over the course of the experiment (Delforge et al., 1999; Christian et al., 2004; Olsson et al., 2004; Slifstein et al., 2004). Based on our results, we feel it is not prohibitive to use two injections from a single synthesis for these experiments though this decision must be determined by the allowable level of variance and the type of analysis being performed. For example, situations that will show limited sensitivity to ligand mass induced variations include experimental designs using each animal as its own control with multiple PET scans (e.g. drug occupancy studies) or when the analysis involves measuring changes in receptor binding with respect to a target region, such as looking for asymmetries in receptor density (Vernaleken et al., 2007; Tomer et al., 2008). For group based comparisons, the effects of radioligand mass should be considered and the experiment should be balanced across cohorts to account for potential mass effects.

Conclusions

We present the measurement of D2/D3 dopamine receptor binding in a large cohort of rhesus monkeys using small animal PET imaging with [F-18]fallypride. The variance of intersubject DVR measured in this cohort was similar across all regions of the brain, with the highest variability found in the caudate nucleus. This variability was consistent with levels reported by others in normative groups measuring PET neuroreceptor binding in humans. Other than the pituitary, there was no significant dependence of D2/D3 binding with sex or age. This presentation focused on methodological issues specific to large cohort studies using small animal PET systems, however, these issues are readily extendable to human studies, particularly with high affinity PET neuroligands. A constant amount of radioactivity was selected for injection rather than basing it on animal weight (e.g. mCi/kg) or constant ligand mass. The 5 mCi injection was dictated by statistical requirements needed to yield an acceptable signal in the reference region. There was a wide range of injected fallypride mass across the cohort as the result of exploring the use of sequential injections for a single production batch of radiotracer. The effects of competing unlabeled ligand (fallypride) could only be detected in the selected structures but not uniformly across all regions of the brain with specific D2/D3 binding across the cohort. This suggests the variance attributed to biological differences obscures the effects of ligand mass effects. The level of acceptable variance is dictated by the resources available to the investigator, i.e. an ideal experimental design would involve the determination of B_{max} and K_D of each animal — though the group variance in these measures would require further investigation. We feel single injection measures of DVR or BP provide suitable indicators of D2/D3 receptor binding and will provide a valuable resource for further investigations of longitudinal, behavioral or pharmacological changes in the D2/D3 neuroreceptor system.

Acknowledgments

The authors would like to thank the following for their contributions to this research: Drs. Jim Holden, Kristin Javaras and Howard Rowley for technical discussions; Joseph Hampel, Elizabeth Smith and Aleem Baktiar for data acquisition and processing; H. Van Valkenberg, Tina Johnson, Kyle Meyer, Elizabeth Zao and the staff at the Harlow Center for Biological Psychology and the Wisconsin National Primate Research Center at the University of Wisconsin (RR000167) for nonhuman primate handling. This work was supported by grants MH046729, MH052354, The HealthEmotions Research Institute and Meriter Hospital.

References

Aalto, S., Bruck, A., Laine, M., Nagren, K., Rinne, J.O., 2005. Frontal and temporal dopamine release during working memory and attention tasks in healthy humans: a positron emission tomography study using the high-affinity dopamine D-2 receptor ligand [C-11]FLB 457. J. Neurosci. 25 (10), 2471–2477.

Alexoff, D.L., Vaska, P., Marsteller, D., Gerasimov, T., Li, J., Logan, J., Fowler, J.S., Taintor, N.B., Thanos, P.K., Volkow, N.D., 2003. Reproducibility of C-11-raclopride binding in the rat brain measured with the MicroPET R4: effects of scatter correction and tracer specific activity. J. Nucl. Med. 44 (5), 815–822.

Asselin, M.C., Montgomery, A.J., Grasby, P.M., Hume, S.P., 2007. Quantification of PET studies with the very high-affinity dopamine D-2/D-3 receptor ligand [C-11]FLB 457: re-evaluation of the validity of using a cerebellar reference region. J. Cereb. Blood Flow Metab. 27 (2), 378–392.

Bendriem, B., Townsend, D.W. (Eds.), 1998. The theory and practice of 3D PET. Developments in Nuclear Medicine. Kluwer Academic Publishers, Dordrecht.

Buchsbaum, M.S., Christian, B.T., Lehrer, D.S., Narayanan, T.K., Shi, B.Z., Mantil, J., Kemether, E., Oakes, T.R., Mukherjee, J., 2006. D2/D3 dopamine receptor binding with [F-18]fallypride in thalamus and cortex of patients with schizophrenia. Schizophr. Res. 85 (1–3), 232–244.

Carson, R.E. 1993. PET parameter estimation using linear integration methods: bias and variability considerations. Proceedings of BrainPET '93 AKITA: Quantification of Brain Function, Akita, Japan, Elsevier.

Christian, B.T., Narayanan, T.K., Shi, B.Z., Mukherjee, J., 2000. Quantitation of striatal and extrastriatal D-2 dopamine receptors using PET imaging of [F-18]fallypride in nonhuman primates. Synapse 38 (1), 71–79.

Christian, B.T., Narayanan, T., Shi, B., Morris, E.D., Mantil, J., Mukherjee, J., 2004. Measuring the in vivo binding parameters of [F-18]-fallypride in monkeys using a PET multiple-injection protocol. J. Cereb. Blood Flow Metab. 24 (3), 309–322.

Christian, B.T., Lehrer, D.S., Shi, B.Z., Narayanan, T.K., Strohmeyer, P.S., Buchsbaum, M.S., Mantil, J.C., 2006. Measuring dopamine neuromodulation in the thalamus: using [F-18] fallypride PET to study dopamine release during a spatial attention task. Neuroimage 31 (1), 139–152.

Colman, R.J., Kemnitz, J.W., 1999. Aging experiments using nonhuman primates. In: Yu, B.P. (Ed.), Methods in Aging Research. CRC Press, Boca Raton.

Costes, N., Merlet, I., Ostrowsky, K., Faillenot, I., Lavenne, F., Zimmer, L., Ryvlin, P., Le Bars, D., 2005. A F-18-MPPF PET normative database of 5-HT1A receptor binding in men and women over aging. J. Nucl. Med. 46 (12), 1980–1989.

Delforge, J., Bottlaender, M., Loc'h, C., Guenther, I., Fuseau, C., Bendriem, B., Syrota, A., Maziere, B., 1999. Quantitation of extrastriatal D2 receptors using a very high-affinity ligand (FLB 457) and the multi-injection approach. J. Cereb. Blood Flow Metab. 19 (5), 533–546.

Emborg, M.E., 2007. Nonhuman primate models of Parkinson's disease. Ilar J. 48 (4), 339–355.

Farde, L., Hall, H., Pauli, S., Halldin, C., 1995. Variability in D-2-dopamine receptor density and affinity — a PET study with [C-11] raclopride in man. Synapse 20 (3), 200–208.

Fox, J.G., Anderson, L.C., Loew, F.M., Quimby, F.W. (Eds.), 2002. Laboratory animal medicine (2nd Edition). American College of Laboratory Animal Medicine Series. American Press, Amsterdam.

Gilbert, D.L., Christian, B.T., Gelfand, M.J., Shi, B., Mantil, J., Sallee, F.R., 2006. Altered mesolimbocortical and thalamic dopamine in Tourette syndrome. Neurology 67 (9), 1695–1697.

Halldin, C., Farde, L., Hogberg, T., Mohell, N., Hall, H., Suhara, T., Karlsson, P., Nakashima, Y., Swahn, C.G., 1995. Carbon-11-Flb-457 — a radioligand for extrastriatal D2 dopamine-receptors. J. Nucl. Med. 36 (7), 1275–1281.

Holden, J.E., Jivan, S., Ruth, T.J., Doudet, D.J., 2002. In vivo receptor assay with multiple ligand concentrations: an equilibrium approach. J. Cereb. Blood Flow Metab. 22 (9), 1132–1141.

Hume, S.P., Gunn, R.N., Jones, T., 1998. Pharmacological constraints associated with positron emission tomographic scanning of small laboratory animals. Eur. J. Nucl. Med. 25 (2), 173–176.

Ichise, M., Ballinger, J.R., Golan, H., Vines, D., Luong, A., Tsai, S., Kung, H.F., 1996. Noninvasive quantification of dopamine D2 receptors with iodine-123-IBF SPECT. J. Nucl. Med. 37 (3), 513–520.

Ichise, M., Toyama, H., Innis, R.B., Carson, R.E., 2002. Strategies to improve neuroreceptor parameter estimation by linear regression analysis. J. Cereb. Blood Flow Metab. 22 (10), 1271–1281.

Ichise, M., Liow, J.S., Lu, J.Q., Takano, T., Model, K., Toyama, H., Suhara, T., Suzuki, T., Innis, R.B., Carson, T.E., 2003. Linearized reference tissue parametric imaging methods: application to [C-11]DASB positron emission tomography studies of the serotonin transporter in human brain. J. Cereb. Blood Flow Metab. 23 (9), 1096–1112.

Ito, H., Takahashi, H., Arakawa, R., Takano, H., Suhara, T., 2008. Normal database of dopaminergic neurotransmission system in human brain measured by positron emission tomography. Neuroimage 39 (2), 555–565.

Jagoda, E.M., Vaquero, J.J., Seidel, J., Green, M.V., Eckelman, W.C., 2004. Experiment assessment of mass effects in the rat: implications for small animal PET imaging. Nucl. Med. Biol. 31 (6), 771–779.

Kaasinen, V., Nagren, K., Hietala, J., Oikonen, V., Vilkman, H., Farde, L., Halldin, C., Rinne, J.O., 2000. Extrastriatal dopamine D2 and D3 receptors in early and advanced Parkinson's disease. Neurology 54 (7), 1482–1487.
Kaasinen, V., Aalto, S., Nagren, K., Rinne, J.O., 2004. Insular dopamine D-2 receptors and novelty seeking personality in Parkinson's disease. Mov. Disord. 19 (11), 1348–1351.
Kalin, N.H., Shelton, S.E., Fox, A.S., Oakes, T.R., Davidson, R.J., 2005. Brain regions associated with the expression and contextual regulation of anxiety in primates. Biol. Psychiatry 58 (10), 796–804.
Kalin, N.H., Shelton, S.E., Fox, A.S., Rogers, J., Oakes, T.R., Davidson, R.J., 2008. The serotonin transporter genotype is associated with intermediate brain phenotypes that depend on the context of eliciting stressor. Molecular Psychiatry 13, 1021–1027.
Kessler, R.M., Whetsell, W.O., Ansari, M.S., Votaw, J.R., Depaulis, T., Clanton, J.A., Schmidt, D.E., Mason, N.S., Manning, R.G., 1993. Identification of extrastriatal dopamine D2 receptors in postmortem human brain with [I-125] epidepride. Brain Res. 609 (1–2), 237–243.
Klimke, A., Larisch, R., Janz, A., Vosberg, H., Muller-Gartner, H.W., Gaebel, W., 1999. Dopamine D-2 receptor binding before and after treatment of major depression measured by [I-123]IBZM SPECT. Psychiatry Research-Neuroimaging 90 (2), 91–101.
Kung, M.P., Kung, H.F., 2005. Mass effect of injected dose in small rodent imaging by SPECT and PET. Nucl. Med. Biol. 32 (7), 673–678.
Lambrecht, R., Eckelman, W.C. (Eds.), 1983. Animal Models in Radiotracer Design. Springer Verlag, New York.
Lancaster, J.L., Tordesillas-Gutierrez, D., Martinez, M., Salinas, F., Evans, A., Zilles, K., Mazziotta, J.C., Fox, P.T., 2007. Bias between MNI and talairach coordinates analyzed using the ICBM-152 brain template. Human Brain Mapping 28, 1194–1205.
Lee, C.M., Farde, L., 2006. Using positron emission tomography to facilitate CNS drug development. Trends Pharmacol. Sci. 27 (6), 310–316.
Lipska, B.K., Weinberger, D.R., 2003. Animal models of schizophrenia. In: Hirsch, S.R., Weinberger, D.R. (Eds.), Schizophrenia. Blackwell Science, Malden, MA, pp. 388–402.
Logan, J., Fowler, J.S., Volkow, N.D., Wang, G.J., Ding, Y.S., Alexoff, D.L., 1996. Distribution volume ratios without blood sampling from graphical analysis of PET data. J. Cereb. Blood Flow Metab. 16 (5), 834–840.
Logan, J., Volkow, N.D., Fowler, J.S., Wang, G.J., Fischman, M.W., Foltin, R.W., Abumrad, N.N., Vitkun, S., Gatley, S.J., Pappas, N., Hitzemann, R., Shea, C.E., 1997. Concentration and occupancy of dopamine transporters in cocaine abusers with [C-11]cocaine and PET. Synapse 27 (4), 347–356.
McLaren, D.G., Kosmatka, K.J., Oakes, T.R., Kroenke, C.D., Kohama, S.G., Matochik, J.A., Ingram, D.K., Johnson, S.C., in press. A population-average MRI-based atlas collection of the rhesus macaque. NeuroImage. doi:10.1016/j.neuroimage.2008.10.058.
Meikle, S.R., Eberl, S., Fulton, R.R., Kassiou, M., Fulham, M.J., 2000. The influence of tomograph sensitivity on kinetic parameter estimation in positron emission tomography imaging studies of the rat brain. Nucl. Med. Biol. 27 (6), 617–625.
Mukherjee, J., Yang, Z.Y., Das, M.K., Brown, T., 1995. Fluorinated benzamide neuroleptics.3. development of (S)-N-[(1-allyl-2-pyrrolidinyl)methyl]-5-(3-[F-18] fluoropropyl)-2,3-dimethoxybenzamide as an improved dopamine D-2 receptor tracer. Nucl. Med. Biol. 22 (3), 283–296.
Mukherjee, J., Yang, Z.Y., Brown, T., Lew, R., Wernick, M., Ouyang, X.H., Yasillo, N., Chen, C.T., Mintzer, R., Cooper, M., 1999. Preliminary assessment of extrastriatal dopamine D-2 receptor binding in the rodent and nonhuman primate brains using the high affinity radioligand, F-18-fallypride. Nucl. Med. Biol. 26 (5), 519–527.
Mukherjee, J., Christian, B.T., Dunigan, K.A., Shi, B.Z., Narayanan, T.K., Satter, M., Mantil, J., 2002. Brain imaging of F-18-fallypride in normal volunteers: blood analysis, distribution, test–retest studies, and preliminary assessment of sensitivity to aging effects on dopamine D-2/D-3 receptors. Synapse 46 (3), 170–188.
Nader, M.A., Czoty, P.W., 2008. Brain imaging in nonhuman primates: insights into drug addiction. Ilar J. 49 (1), 89–102.
Oakes, T.R., Fox, A.S., Johnstone, T., Chung, M.K., Kalin, N., Davidson, R.J., 2007. Integrating VBM into the general linear model with voxelwise anatomical covariates. Neuroimage 34 (2), 500–508.
Olsson, H., Halldin, C., Swahn, C.-G., Farde, L., 1999. Quantification of [lsqb]11C[rsqb]FLB 457 binding to extrastriatal dopamine receptors in the human brain. J. Cereb. Blood Flow Metab. 19 (10), 1164.
Olsson, H., Halldin, C., Farde, L., 2004. Differentiation of extrastriatal dopamine D2 receptor density and affinity in the human brain using PET. Neuroimage 22 (2), 794–803.
Pani, L., Porcella, A., Gessa, G.L., 2001. Hypothesis testing: dopaminergic system, environmental pressure, and evolutionary mismatch. In: Bolis, C.L., Pani, L., Licinio, J. (Eds.), Dopaminergic System: Evolution from Biology to Clinical Aspects. Lippincott Williams & Wilkins Healthcare, Philadelphia, pp. 1–15.
Paxinos, G., Huang, X.F., Toga, A.W., 2000. The Rhesus Monkey Brain in Sterotaxic Coordinates. Academic Press, San Diego.
Porrino, L.J., Daunais, J.B., Smith, H.R., Nader, M.A., 2004. The expanding effects of cocaine: studies in a nonhuman primate model of cocaine self-administration. Neurosci. Biobehav. Rev. 27 (8), 813–820.
Rabiner, E.A., Messa, C., Sargent, P.A., Husted-Kjaer, K., Montgomery, A., Lawrence, A.D., Bench, C.J., Gunn, R.N., Cowen, P., Grasby, P.M., 2002. A database of [C-11]WAY-100635 binding to 5-HT1A receptors in normal male volunteers: normative data and relationship to methodological, demographic, physiological, and behavioral variables. Neuroimage 15 (3), 620–632.
Riccardi, P., Zald, D., Li, R., Park, S., Ansari, M.S., Dawant, B., Anderson, S., Woodward, N., Schmidt, D., Baldwin, R., Kessler, R., 2006. Sex differences in amphetamine-induced displacement of [F-18] fallypride in striatal and extrastriatal regions: a PET study. Am. J. Psychiatr. 163 (9), 1639–1641.
Rieck, R.W., Ansari, M.S., Whetsell, W.O., Deutch, A.Y., Kessler, R.M., 2004. Distribution of dopamine D-2-like receptors in the human thalamus: autoradiographic and PET studies. Neuropsychopharmacology 29 (2), 362–372.
Roberts, A.D., Moor, C.F., DeJesus, O.T., Barnhart, T.E., Larson, J.A., Mukherjee, J., Nickles, R.J., Schueller, M.J., Shelton, S.E., Schneider, M.L., 2004. Prenatal stress, moderate fetal alcohol, and dopamine system function in rhesus monkeys. Neurotoxicol. Teratol. 26 (2), 169–178.
Siessmeier, T., Zhou, Y., Buchholz, H.G., Landvogt, C., Vernaleken, I., Piel, M., Schirrmacher, R., Rosch, F., Schreckenberger, M., Wong, D.F., Cumming, P., Grunder, G., Bartenstein, P., 2005. Parametric mapping of binding in human brain of D-2 receptor ligands of different affinities. J. Nucl. Med. 46 (6), 964–972.
Slifstein, M., Hwang, D.R., Huang, Y.Y., Guo, N.N., Sudo, Y., Narendran, R., Talbot, P., Laruelle, M., 2004. In vivo affinity of [F-18]fallypride for striatal and extrastriatal dopamine D-2 receptors in nonhuman primates. Psychopharmacology 175 (3), 274–286.
Smith, S.M., Jenkinson, M., Woolrich, M.W., Beckmann, C.F., Behrens, T.E.J., Johansen-Berg, H., Bannister, P.R., De Luca, M., Drobnjak, I., Flitney, D.E., Niazy, R.K., Saunders, J., Vickers, J., Zhang, Y.Y., De Stefano, N., Brady, J.M., Matthews, P.M., 2004. Advances in functional and structural MR image analysis and implementation as FSL. Neuroimage 23, S208–S219.
Sossi, V., Camborde, M.L., Tropini, G., Newport, D., Rahmim, A., Doudet, D.J., Ruth, T.J., 2005. The influence of measurement uncertainties on the evaluation of the distribution volume ratio and binding potential in rat studies on a microPET (R) R4: a phantom study. Phys. Med. Biol. 50 (12), 2859–2869.
Strome, E.M., Doudet, D.J., 2007. Animal models of neurodegenerative disease: insights from in vivo imaging studies. Mol. Imaging biol. 9 (4), 186–195.
Suhara, T., Okubo, Y., Yasuno, F., Sudo, Y., Inoue, M., Ichimiya, T., Nakashima, Y., Nakayama, K., Tanada, S., Suzuki, K., Halldin, C., Farde, L., 2002. Decreased dopamine D-2 receptor binding in the anterior cingulate cortex in schizophrenia. Arch. Gen. Psychiatry 59 (1), 25–30.
Talvik, M., Nordstrom, A.L., Olsson, H., Halldin, C., Farde, L., 2003. Decreased thalamic D-2/D-3 receptor binding in drug-naive patients with schizophrenia: a PET study with [C-11]FLB 457. Int. J. Neuropsychopharmacol. 6 (4), 361–370.
Tomer, R., Goldstein, R.Z., Wang, G.J., Wong, C., Volkow, N.D., 2008. Incentive motivation is associated with striatal dopamine asymmetry. Biol. Psychol. 77 (1), 98–101.
Tuppurainen, H., Kuikka, J., Viinamaki, H., Husso-Saastamoinen, M., Bergstrom, K., Tiihonen, J., 2003. Extrastriatal dopamine D-2/3 receptor density and distribution in drug-naive schizophrenic patients. Mol. Psychiatry 8 (4), 453–455.
Vernaleken, I., Weibrich, C., Siessmeier, T., Buchholz, H.G., Rosch, F., Heinz, A., Cumming, P., Stoeter, P., Bartenstein, P., Grunder, G., 2007. Asymmetry in dopamine D-2/3 receptors of caudate nucleus is lost with age. Neuroimage 34 (3), 870–878.
Worsley, K.J., Evans, A.C., Marrett, S., Neelin, P., 1992. A 3-dimensional statistical-analysis for Cbf activation studies in human brain. J. Cereb. Blood Flow Metab. 12 (6), 900–918.
Yasuno, F., Suhara, T., Okubo, Y., Sudo, Y., Inoue, M., Ichimiya, T., Takano, A., Nakayama, K., Haildin, C., Farde, L., 2004. Low dopamine D-2 receptor binding in subregions of the thalamus in schizophrenia. Am. J. Psychiatr. 161 (6), 1016–1022.
Zabavnik, J., Wu, W.X., Eidne, K.A., McNeilly, A.S., 1993. Dopamine-D(2) receptor messenger-RNA in the pituitary during the estrous-cycle, pregnancy and lactation in the rat. Mol. Cell. Endocrinol. 95 (1–2), 121–128.
Zhou, Y., Endres, C.J., Brasic, J.R., Huang, S.C., Wong, D.F., 2003. Linear regression with spatial constraint to generate parametric images of ligand-receptor dynamic PET studies with a simplified reference tissue model. Neuroimage 18 (4), 975–989.